JOURNAL OF THE GEOTECHNICAL ENGINEERING DIVISION

Risk Analysis for Ground Failure by Liquefaction[a]

By Mishac K. Yegian,[1] A. M. ASCE and Robert V. Whitman,[2] F. ASCE

Introduction

Among the causes of earthquake-induced ground failure is liquefaction of saturated cohesionless materials. Many failures of bridge piers, embankments, quaywalls, buildings, and slopes during past earthquakes have been attributed to liquefaction of foundation soils (9,15,17). Laboratory tests have led to a general understanding of the phenomenon: back-and-forth shearing causes excess pore pressures that in turn cause a decrease in shearing resistance. The likelihood of liquefaction increases with increasing intensity and number of cycles of back-and-forth shearing (16).

This paper describes a procedure for estimating the overall probability of ground failure at a site by liquefaction, taking into account both the probability of an earthquake occurring and the probability of that earthquake causing ground failure by liquefaction. For a given earthquake, the probability of liquefaction can be expressed very simply as

$$P_E[F_L] = P[F_L|E]\ P[E] \qquad (1)$$

in which $P_E[F_L]$ is the overall probability of liquefaction of some site during the earthquake E; $P[F_L|E]$ is the probability of liquefaction at the site given that the earthquake E occurs; and $P[E]$ is the probability that the earthquake E occurs. The total overall probability of liquefaction at the site is obtained by summing over all possible earthquakes:

Note.—Discussion open until December 1, 1978. To extend the closing date one month, a written request must be filed with the Editor of Technical Publications, ASCE. This paper is part of the copyrighted Journal of the Geotechnical Engineering Division, Proceedings of the American Society of Civil Engineers, Vol. 104, No. GT7, July, 1978. Manuscript was submitted for review for possible publication on August 2, 1977.

[a]Presented at October 17–21, 1977, ASCE Annual Convention Exposition and Continuing Education Program, held at San Francisco, Calif. (Preprint 2913).

[1]Asst. Prof. of Civ. Engrg., Northeastern Univ., Boston, Mass.

[2]Prof. of Civ. Engrg., Massachusetts Inst. of Tech., Cambridge, Mass.

$$P[F_L] = \sum_{E} P[F_L|E]\, P[E] \quad \ldots\ldots (2)$$

The evaluation of $P[E]$ falls into the professional discipline of seismology, while the evaluation of $P[F_L|E]$—often referred to as a *conditional probability* of liquefaction—involves geotechnical engineering.

There are a number of ways in which the earthquake may be characterized. One common way is to describe the intensity of shaking at the site by the peak acceleration A and duration D. Thus Eq. 2 would be rewritten as

$$P[F_L] = \sum_{A,D} P[F_L|A,D]\, P[A,D] \quad \ldots\ldots (3)$$

in which $P[F_L|A,D]$ is the conditional probability of liquefaction given that a ground motion characterized by A and D occurs; and $P[A,D]$ is the probability that the motion occurs. The summation is over all possible combinations of A and D. $P[A,D]$ might be evaluated by seismic risk analysis (1,6) although no procedure now exists for evaluating the probability of the joint occurrence of A and D. Eq. 3 may be expanded so as to evaluate $P[A,D]$ in two steps:

$$P[F_L] = \sum_{M,R} P[F_L|A,D]\, P[A,D|M,R]\, P[M,R] \quad \ldots\ldots (4)$$

in which $P[A,D|M,R]$ is an attenuation law giving the probability of experiencing a ground motion with A and D at the site given that an earthquake with magnitude M occurs with hypocentral distance R to the site; and $P[M,R]$ is the probability that an earthquake with M and R occurs. Now the summation is over all possible combinations of M and R. An alternative procedure omits the intermediate step of the attenuation law:

$$P[F_L] = \sum_{M,R} P[F_L|M,R]\, P[M,R] \quad \ldots\ldots (5)$$

in which $P[F_L|M,R]$ is the conditional probability of liquefaction, given an earthquake with magnitude M at hypocentral distance R from the site. The uncertainty in the attenuation law now is incorporated into the conditional probability. Studies using Eqs. 3 or 4, where the earthquake is represented by the intensity of shaking at the site, will hereafter be referred to as *A & D approaches*. Studies using Eq. 5, where the earthquake is represented by the magnitude and hypocentral distance, will be called *M & R approaches*.

Relation to Conventional Practice.—In usual practice, A and D are fixed, and a site is investigated—and corrective action is taken if necessary—to ensure that $P[F_L|A,D]$ is sufficiently small. Typically this is achieved by adopting a safety factor upon the resistance of the soil to liquefaction. Much work has gone into the development of theoretical and empirical procedures for evaluation of liquefaction potential at a site (4,12,13,18,20). This conventional practice is convenient from an administrative viewpoint: it permits the seismologist and the geotechnical engineer to develop separate standards of practice for the two aspects of the problem. From the standpoint of balancing safety and economy, however, the separation is unfortunate. Frequently, both the seismologist and the geotechnical engineer are conservative in their separate parts, with a resulting overall conservatism that is excessive. Sometimes $P[A,D]$ and $P[F_L|A,D]$ are estimated for the specified A and D, and multiplied to give an estimate of the overall risk—as in Eq. 1. Such an estimate can, however, be very misleading unless the risk is summed over all possible values of A and D—as in Eq. 3. For example, an earthquake shaking stronger than the shaking specified for design has a smaller probability of occurring but $P[F_L|A,D]$ will be larger, and their product may contribute to the overall risk.

With the present knowledge, neither $P[F_L|E]$ nor $P[E]$ can be estimated accurately, and accurate estimates of the overall risk are not possible. Nonetheless, crude computations of risk have proved quite useful in assessing the relative risk of earthquake-induced failure among various types of buildings and in comparing earthquake risks with risks from other natural disasters (21). There are many potential benefits in describing the risk of ground failure by liquefaction in this same way.

***M & R* Versus *A & D* Approaches.**—The intensity of shaking at a site is described by the magnitude and hypocentral distance of the design earthquake. This is especially true for cases where a seismic risk analysis is performed for the region around the site to arrive at some design earthquake intensity at the site. In view of the fact that most current analyses for liquefaction employ acceleration and duration, the need to estimate these design parameters from the magnitude of the postulated earthquake for liquefaction studies becomes essential. The acceleration value is commonly estimated using an attenuation law and the magnitude and hypocentral distance of the chosen earthquake (8). The duration of the earthquake shaking, which is usually expressed in terms of the parameter N_{eq} referred to as the number of equivalent significant cycles, is also estimated from the magnitude of the earthquake using some empirical procedure (14).

It has been recognized that the use of acceleration and duration, to both develop an analysis for liquefaction and to study liquefaction potential employing such an analysis, involves uncertainties (5,22). An alternate method for study of liquefaction potential is proposed herein, based on interpretation of field observations in terms of earthquake magnitude and hypocentral distance. The benefits of choosing magnitude and distance to describe an earthquake intensity in liquefaction studies are manifold. Use of earthquake magnitude in liquefaction analysis accounts for duration more directly than the empirical parameter N_{eq}, which can only be used together with acceleration. The earthquake magnitude and hypocentral distance for a case history are more readily and accurately estimated than the acceleration level and its duration, expecially if the acceleration is to be estimated using an attenuation law. Therefore, the use of magnitude and distance creates greater opportunities for accumulating case histories. Sites where liquefaction did occur but unfortunately no measures of the accelerations were available can be now included in the investigations. Also numerous sites where liquefaction did not occur can now be considered in studies of case histories to develop a reliable criterion for soil liquefaction as it happens in the field.

Finally, a liquefaction analysis technique that employs magnitude and distance can be incorporated directly into a risk analysis yielding the total overall probability of liquefaction, as shown in Eq. 5, without the use of the highly uncertain attenuation law shown in Eq. 4.

This paper presents a risk analysis for estimating the likelihood of earthquake-induced ground failure by liquefaction. First, to evaluate $P[F_L|M,R]$ an empirical expression characterizing the resistance of a site to liquefaction is developed from observations of liquefaction and nonliquefaction during actual earthquakes. Then, using a simple procedure commonly used in seismic risk analysis, the conditional probability $P[F_L|M,R]$ is combined with $P[M,R]$ to estimate the overall risk. An example is worked through in detail.

A comparable risk analysis for liquefaction that employs the *A & D* approach previously described has also been developed. The results will be published in a later paper.

M & R Approach to Interpretation of Field Data

Having preferred to perform the liquefaction risk analysis in terms of magnitude and distance, it is necessary to develop a probabilistic model that also employs these seismic parameters to yield the likelihood of liquefaction given a certain level of earthquake shaking. The model developed for this purpose and presented herein is based on the interpretation of case history data.

To interpret the field data, a parameter S_c was employed, having the form:

$$S_c = \frac{e^{aM} H}{(R+16)^b \bar{\sigma}_v} \quad \ldots\ldots (6)$$

in which M is the earthquake magnitude on the Richter scale; R is the hypocentral distance, in miles; H is the depth to the point of interest, in feet; and $\bar{\sigma}_v$ is the vertical effective stress at this same point, in pounds per square inch. This parameter is proportional to the ratio of earthquake-induced shear stress to vertical effective stress. Use of the quantity $e^{aM}/(R+16)^b$ is suggested by attenuation laws for ground motions (8,11). A range of values for the constants a and b was chosen by examining proposed attenuation laws for acceleration at bedrock, and studying theoretically the change in acceleration between bedrock and ground surface. Several different sets of values were used to fit a curve, such as Fig. 1, through field data. Finally it was concluded that $a = 0.5$ and $b = 1$ were the most appropriate values, so that Eq. 6 became:

$$S_c = \frac{e^{0.5M} H}{(R+16)\bar{\sigma}_v} \quad \ldots\ldots (7)$$

These parametric studies were also used to suggest suitable values for the variance in S_c.

The parameter S_c described in Eq. 7 was employed to interpret the case histories reported earlier by Seed and Idriss (18), Castro (4), and a few Japanese sites where liquefaction was not observed (10). The results of the study are presented in Fig. 1. The horizontal axis in this figure represents the SPT values corrected for the overburden pressure using (4)

$$N' = \frac{50N}{\bar{\sigma}_v + 10} \quad \ldots\ldots (8)$$

in which N is the number of blows per foot; and $\bar{\sigma}_v$ is the vertical effective stress, in pounds per square inch.

In Fig 1 the solid circles correspond to sites where liquefaction was observed and conversely the open circles signify no liquefaction. The data in Fig. 1 appear to plot over the entire area bounded by the axes of the figure. This should not be categorically considered as scatter. What it implies is that if during an earthquake of a certain magnitude a sand deposit liquefied it would have also liquefied during any other larger magnitude earthquake. To develop a criterion for liquefaction as a function of soil density expressed in terms of corrected blow counts N', it is necessary to define a boundary line separating, with some confidence, the solid circles establishing a zone of probable liquefaction from the open circles establishing a zone of no liquefaction. This problem is commonly referred to in statistics as "pattern recognition." In short, the criterion sought should be in the form of a plot that is defined ideally by the lowest possible position that any solid circle would assume or the highest possible position that any open circle would assume.

A number of techniques have been developed in statistics to study patterns of different behaviors very similar to the problem described in the preceding

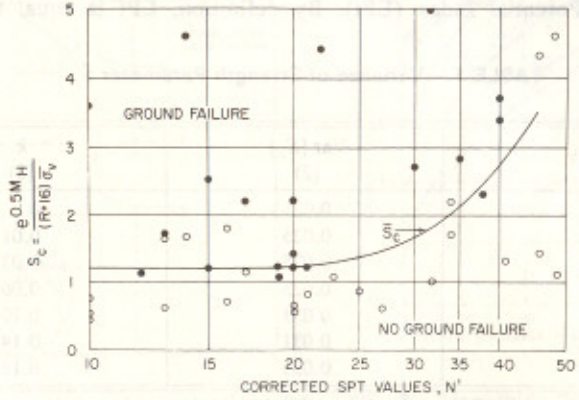

FIG. 1.—Average Strength Parameter $\bar{S}_c$

paragraph (2,5,19). However, a careful study revealed the inapplicability of these techniques to the problemiof liquefaction versus no liquefaction. Therefore, a rather simplified approach was developed to statistically determine the line separating the solid circles from the open circles of Fig. 1. The method is termed "least square of misclassified points." The method consists of locating the boundary line such that the sum of the squares of the distances of the misclassified points from the boundary line is a minimum. The misclassified points are the solid circles that plot below the line in the region of no liquefaction and the open circles that plot above the line in the region of liquefaction.

The process of establishing a criterion such as shown in Fig. 1 involves several sources of uncertainties. An attempt was made to identify the major sources of uncertainties, to quantify them, and finally to incorporate them into the variance of $\bar{S}_c$. Some of the sources of uncertainties considered are: (1) Form of the parameter $\bar{S}_c$ due to uncertainties in the values of the coefficients a and b; (2) location of the boundary line separating the solid circles from the

open circles in Fig. 1 due to the simplified method used; and (3) parameters M, R, and N' for each case history.

Considering these sources of uncertainties, an average strength parameter, $\bar{S}_c$, defining liquefaction or no liquefaction and its variance were estimated. Table 1 presents the variance of $\bar{S}_c$ for different values of N'. Fig. 1 shows the average strength parameter $\bar{S}_c$.

In as much as most of the case histories studied herein corresponded to soils characterized as uniformly graded, fine to medium sands and silty sands, the plot of Fig. 1 and conclusions based on this plot are only valid for similar types of soil. Also, since only a few case histories are available where liquefaction did occur at large values of N', a caution is made about the reliability of that portion of the plot in Fig. 1 where N' is greater than 30.

Conditional Probability of Liquefaction

For the sake of mathematical simplicity in the probabilistic analysis developed herein, a new measure of liquefaction potential of a sand is defined, i.e., Liquefaction Potential Index (LPI). By definition, LPI is equal to the ratio

TABLE 1.—Variance of Strength Parameter $\bar{S}_c$

N' (1)	Var $[\bar{S}_c]$ (2)	k (3)
10	0.025	0
20	0.025	0.01
25	0.025	0.03
30	0.025	0.06
35	0.031	0.10
40	0.031	0.14
45	0.031	0.18

of the shear stresses caused by an earthquake shaking to the resistance of the sand to such shaking. Therefore

$$\text{LPI} = \frac{(\tau)_{\text{earthquake}}}{(\tau)_{\text{strength}}} \quad \ldots\ldots (9)$$

Liquefaction failure of a sand deposit is expected to occur whenever the earthquake-induced stresses are greater than the available shear strength of the sand. Therefore:

$$\text{LPI} > 1.0 \quad \text{liquefaction expected} \quad \ldots\ldots (10)$$

$$\text{LPI} < 1.0 \quad \text{liquefaction not expected} \quad \ldots\ldots (11)$$

Since the parameter S_c expressed in Eq. 7 is proportional to shear stresses causing liquefaction, the plot of $\bar{S}_c$ shown in Fig. 1 is proportional to the average shear strength of soils against liquefaction. Employing the definition of Liquefaction Potential Index, the average LPI is

$$\overline{\text{LPI}} = \frac{(S_c)_{\text{earthquake}}}{\bar{S}_c} \quad \ldots\ldots (12)$$

in which $(S_c)_{\text{earthquake}}$ is given by Eq. 7 and $\bar{S}_c$ is given by the plot of Fig. 1. Substituting for the parameter $(S_c)_{\text{earthquake}}$:

$$\overline{\text{LPI}} = \frac{e^{0.5M} H}{(R + 16)\bar{\sigma}_v \bar{S}_c} \quad \ldots\ldots (13)$$

Eq. 13 expresses the average computed LPI as a function of the earthquake intensity and average soil strength parameter, $\bar{S}_c$. However, because of uncertainties in the parameters that are used to compute LPI and especially uncertainty in the strength parameter $\bar{S}_c$, the actual LPI might be lower of higher than the average computed LPI. Thus, accounting for these uncertainties, a statement can be made regarding the probability of liquefaction at a site.

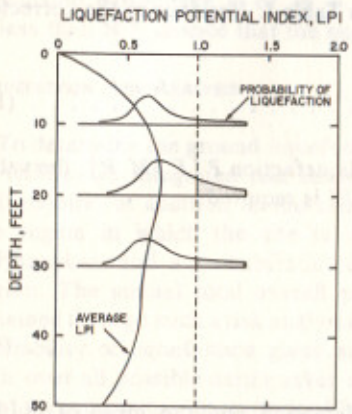

FIG. 2.—Probability of Liquefaction with Depth

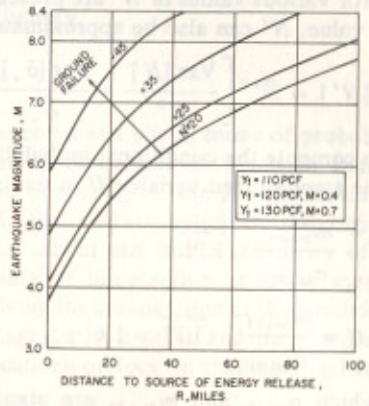

FIG. 3.—Magnitude-Distance Relationships for Water Table at Ground Surface and for 50% Probability of Liquefaction

Liquefaction potential of a sand deposit may therefore be described in a probabilistic manner as the probability of having the actual LPI exceeding or equal to 1.0:

$$P[F_L|M,R] = P[\text{LPI} \geq 1.0|M,R] \quad \ldots\ldots (14)$$

To compute this conditional probability of liquefaction one is required to estimate the variance of LPI and then employ a probability density function for LPI. The area under the probability density function for LPI $\geq$ 1.0 will yield the probability of liquefaction. Fig. 2 describes schematically the probability of liquefaction computations for different depths assuming a lognormal distribution for LPI. Benjamin and Cornell (3) describe the lognormal distribution as being best to represent a phenomenon arising from multiplicative mechanisms such as depicted in the expression for LPI. It is emphasized herein that the assumption of lognormal distribution for LPI, while it may be reasonable for

intermediate ranges of probability calculations, involves great uncertainties when these calculations are made using the tail ends of the distribution.

Variance of LPI.—For a given earthquake intensity defined by magnitude M and hypocentral distance R, the coefficient of variation of LPI can be approximated by (3)

$$V_{LPI} = \left[\frac{\text{Var}[\bar{\sigma}_v]}{\bar{\sigma}_v^2} + \frac{\text{Var}[\bar{S}_c]}{\bar{S}_c^2}\right]^{1/2} \quad \ldots\ldots (15)$$

The total variance of $\bar{S}_c$ should include the variance of $\bar{S}_c$ from Table 1 and the uncertainty in the corrected blow counts, N'. The total variance of $\bar{S}_c$ can be approximated by

$$\text{Var}[\bar{S}_c] = \text{Var}[\bar{S}_c]_{N'} + k^2 \text{Var}[N'] \quad \ldots\ldots (16)$$

in which $\text{Var}[\bar{S}_c]_{N'}$ is the variance of $\bar{S}_c$ given N'; and k is the slope of the average strength curve of Fig. 1 plotted on an arithmetic scale. Values of k for various values of N' are presented in Table 1. Variance of the corrected SPT value, N' can also be approximated by

$$\text{Var}[N'] = \bar{N}'^2 \left[\frac{\text{Var}[N]}{N^2} + \frac{\text{Var}[\bar{\sigma}_v]}{\bar{\sigma}_v^2}\right] \quad \ldots\ldots (17)$$

To compute the conditional probability of liquefaction $P[F_L|M,R]$, the value of the standardized variable U in terms of LPI is required:

$$U = -\frac{m_{\ln LPI}}{\sigma_{\ln LPI}}; \quad \overline{LPI} \le 1.0 \quad \ldots\ldots (18)$$

$$\text{or} \quad U = \frac{m_{\ln LPI}}{\sigma_{\ln LPI}}; \quad \overline{LPI} > 1.0 \quad \ldots\ldots (19)$$

in which $\sigma_{\ln LPI}$ and $m_{\ln LPI}$ are standard deviation and the mean of ln LPI, respectively, and are

$$\sigma^2_{\ln LPI} = \ln[V^2_{LPI} + 1] \quad \ldots\ldots (20)$$

$$\text{and} \quad m_{\ln LPI} = \ln \overline{LPI} - \frac{1}{2}\sigma^2_{\ln LPI} \quad \ldots\ldots (21)$$

Therefore, for a given average LPI and its coefficient of variation V_{LPI}, substituting Eqs. 20 and 21 into Eqs. 18 and 19 to estimate U and entering standard normal tables, the conditional probability of liquefaction can be determined.

Preliminary Analysis for Liquefaction Potential

The strength plot of Fig. 1 can be employed to develop charts that might be used to obtain preliminary estimates of the liquefaction potential at a site. Employing the definition of average liquefaction potential index, $\overline{LPI}$, magnitude-distance relationships can be developed to determine the liquefaction potential at a site under average conditions. Referring to Eq. 13, the desired magnitude-distance relationship can be expressed by

$$M = 2 \ln\left[\frac{(R+16)\bar{\sigma}_v \bar{S}_c}{H}\right] \quad \ldots\ldots (22)$$

Fig. 3 shows plots of earthquake magnitude versus distance to source of energy release for a "typical" site where the water table is at the ground surface. The plots shown are only valid for an assumed total unit weight equal to 110 pcf (1.75×10^3 kg/m^3). For γ_t = 120 pcf or 130 pcf (1.92×10^3 kg/m^3 or 2.08×10^3 kg/m^3) the earthquake magnitude obtained from Fig. 3 should be increased by 0.4 and 0.7, respectively.

The plots shown in Fig. 3 could be used for preliminary studies as follows. As an example, consider a site where the water table is at the ground surface, the average corrected blow counts $\bar{N}'$ = 25 and γ_t = 110 pcf (1.75×10^3 kg/m^3). If the postulated earthquake is of a magnitude equal to 7.0 and the hypocentral distance = 40 miles (64 km), there is greater than 50% chance that liquefaction will occur during the postulated earthquake. However, if the postulated earthquake is of M = 7.0 and R = 60 miles (96 km), then there is less than 50% chance that the site will liquefy.

Liquefaction Risk Analysis

To determine the ground liquefaction potential at a site in terms of probability of failure, an integrated risk analysis should be conducted. Such an analysis will require, in addition to the conditional probabilities, the seismic history of the region in which the site is located, the characteristics of the regional earthquakes, and a probabilistic prediction about the future seismicity of the region. The annual total overall probability of liquefaction at a site may be obtained through such a risk analysis, involving the computation of the conditional probability of liquefaction given an earthquake at a point and the integration of it over all possible earthquakes and locations of foci. In mathematical form, this integration may be expressed by

$$P[F_L]/\text{yr} = \int_R \int_M P[F_L|M,R_i,E \text{ at } i]\, f(M)$$

$$P[E \text{ at } i]\, dMdR \quad \ldots\ldots (23)$$

in which i is the location of the focus of a future earthquake; $P[F_L|M,R_i,E$ at $i]$ is the conditional probability of liquefaction given that an earthquake of magnitude M and hypocentral distance R_i occurs at i; $f(M)$ is the probability density function of earthquake magnitude M; and $P[E$ at $i]$ is the annual probability of an earthquake occurring at i.

The probability expression of Eq. 23 is very general and valid for any type of earthquake source. In general the double integration in Eq. 23 can be carried out using any of the procedures employed in seismic risk analysis. In the following section a simplified procedure will be presented for performing the double integration in Eq. 23 assuming a "uniform" circular earthquake source area.

"Uniform" Circular Earthquake Source Area.—Fig. 4 shows a "uniform" circular source area around a site. The characteristic of this source area is that everywhere within the circle, the assumed maximum earthquake magnitude M_1, the minimum earthquake magnitude M_0, the focal depths, d_0, and the

rate of occurrence of earthquakes are the same.

To introduce the required simplification to Eq. 23, it is assumed that the circular source area consists of rings of infinitesimal thickness dr as shown in Fig. 4. These rings extend to a distance r_{max} away from the site beyond which no earthquake of interest $(M < M_1)$ has any significant contribution to the probability of liquefaction at the site.

The computations for the total overall probability of liquefaction at the site shown in Fig. 4 will be very much simplified if first the contribution to the probability of liquefaction of a single ring, say ring i of thickness dr, is computed. Within this ring, all potential earthquakes will have the same focal depth, d_0, and therefore, for all earthquakes, the distance from the focus to the site will be

$$R_i = (r_i^2 + d_0^2)^{1/2} \quad (24)$$

Referring to Eq. 23, the total overall probability equation for the ring of

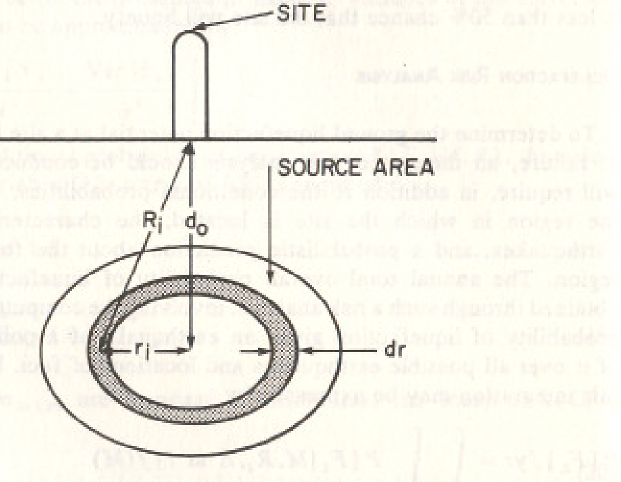

FIG. 4.—Circular "Uniform" Earthquake Source Area

radius r_i, reduces to

$$P[F_L]/\text{yr}_{\text{at } r_i} = \int_{M_0}^{M_1} P[F_L|M, R_i, E \text{ at } i]\, f(M)\, P[E \text{ at } i]\, dM \quad (25)$$

The annual probability of an earthquake occurring within the circular ring of radius r_i can be estimated by

$$P[E \text{ at } i]/\text{yr} = \bar{\lambda}\, 2\pi r_i\, dr \quad (26)$$

in which $\bar{\lambda}$ is the average annual rate of occurrence of earthquakes per unit area of the uniform source. Also, Cornell and Vanmarcke (7) expressed the probability density function of magnitude M by

$$f(M) = K_m \beta \exp[-\beta(M - M_0)] \quad (27)$$

in which β is a magnitude-frequency parameter describing the fraction of earthquakes exceeding a certain magnitude; and K_m is normalizing factor given by

$$K_m = \{1 - \exp[-\beta(M_1 - M_0)]\}^{-1} \quad (28)$$

Substituting Eqs. 26 and 27 into Eq. 25:

$$P[F_L]/\text{yr}_{\text{at } r_i} = \int_{M_0}^{M_1} P[F_L|M, R_i, E \text{ at } i]\, K_m \beta \exp[-\beta(M - M_0)]\, 2\pi \bar{\lambda}\, r_i\, dr\, dM \quad (29)$$

The total overall annual probability of liquefaction is equal to the sum of the contributions from all rings extending from $r = 0$ to $r = r_{max}$. Therefore

$$P[F_L]/\text{yr} = \int_0^{r_{max}} \int_{M_0}^{M_1} P[F_L|M, R_i, E \text{ at } i]\, K_m \beta \exp[-\beta(M - M_0)]\, 2\pi \bar{\lambda}\, r_i\, dr\, dM \quad (30)$$

The conditional probability in Eq. 30 is computed in terms of R_i. Therefore, it is also convenient to express Eq. 30 in terms of R_i and not r_i. Employing Eq. 24, Eq. 30 can be rewritten as

$$P[F_L]/\text{yr} = \int_{d_0}^{R_{max}} \left[\int_{M_0}^{M_1} P[F_L|M, R_i, E \text{ at } i]\, K_m \beta \exp[-\beta(M - M_0)]\, dM \right] 2\pi \bar{\lambda}\, R_i\, dR \quad (31)$$

The inner integral in Eq. 31 is the probability of liquefaction at a site per earthquake per unit area at R_i miles from the site. Since the conditional probability of liquefaction cannot be expressed in mathematically closed form, this inner integral is best evaluated numerically:

$$\text{inner integral} = f(R_i) = K_m \beta \sum_{M_0}^{M_1} P[F_L|M, R_i, E \text{ at } i]\, \exp[-\beta(M - M_0)]\, \Delta M \quad (32)$$

in which ΔM is a small interval of magnitude chosen for the summation. Usually, acceptable accuracy is achieved by choosing $\Delta M = 0.1$–0.2 on the Richter scale.

The outer integral in Eq. 31 sums up the contributions of all the annular source areas with radii varying from $r = 0$ $(R = d_0)$ to $r = r_{max}$ $(R = R_{max})$. The upper limit of the integration, R_{max}, defines the maximum hypocentral distance beyond which the conditional probability of liquefaction for earthquake magnitudes ranging between M_0 and M_1 is insignificant.

Maximum Hypocentral Distance of Interest.—The criterion employed for estimating R_{max} is

$$P[F_L|M_1, R_{max}, E \text{ at } i] = 0.001 \quad (33)$$

Since LPI is assumed to be lognormally distributed, the value of the standardized

variable can be evaluated from Eq. 18. For the criterion expressed in Eq. 33, the value of U from normal tables is estimated to be equal to 3.09. Employing this value of U and the definition of LPI and solving for R_{max}:

$$R_{max} = \frac{\exp\{0.5M_1 + 3.09[\ln(V_{LPI}^2 + 1)]^{1/2}\} H}{\bar{\sigma}_v \bar{S}_c (V_{LPI}^2 + 1)^{1/2}} - 16 \quad \ldots\ldots\ldots\ldots (34)$$

Therefore, the value of R_{max}, among other variables, is a function of V_{LPI}, the coefficient of variation of LPI. Fig. 5 presents plots of R_{max} versus V_{LPI}, for different values of N' and for the case where the water table is at the ground surface and the maximum credible earthquake magnitude, $M_1 = 8.4$. From this figure, it can be seen that the denser the soil, the smaller the distance beyond which earthquakes of magnitude equal to or less than 8.4 are of no concern. Also for a given density, the larger the uncertainty in the soil conditions, the larger is R_{max}. The line of minimum V_{LPI} in Fig. 5 corresponds to uncertainties only due to the average strength parameter $\bar{S}_c$.

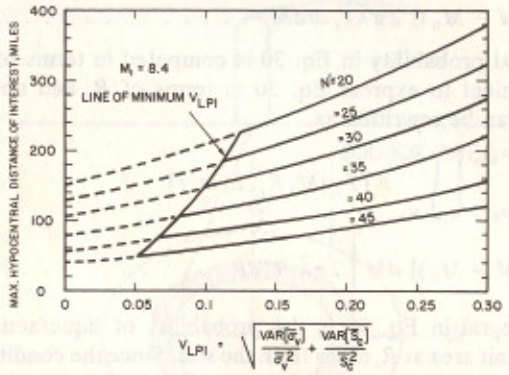

FIG. 5.—Maximum Hypocentral Distance Versus Coefficient of Variation of LPI for Water Table at Ground Surface

Annual Probability of Liquefaction.—The following procedure is recommended for calculating the total overall annual probability of liquefaction for a circular "uniform" source area around a site:

1. Establish the maximum probable earthquake magnitude, M_1, for the region under study. Calculate R_{max} using Eq. 34 and determine the region around the site the seismicity of which is to be studied to estimate the rate of earthquake occurrence, $\bar{\lambda}$, and the magnitude-frequency parameter, β.
2. For various assumed probabilities of liquefaction ranging from ≈0% to ≈100% read off the corresponding values of U from standard normal tables.
3. For each U, calculate $\overline{\text{LPI}}$ using Eqs. 18 or 19.
4. For a specific R_i and for each $\overline{\text{LPI}}$, calculated in Step 3, calculate M by

$$M = 2 \ln \left[\frac{(R_i + 16)\bar{\sigma}_v \bar{S}_c \overline{\text{LPI}}}{H} \right] \quad \ldots\ldots\ldots\ldots\ldots\ldots\ldots\ldots (35)$$

and plot the probability of liquefaction as a function of M.

5. Repeat Step 4 for various values of R_i ranging from d_0–R_{max} to generate conditional probabilities of liquefaction versus magnitude.
6. For each R_i, evaluate the integral presented in Eq. 32 by discretizing the plots generated in Step 4. Plot the values of the integral thus calculated as a function of R_i.
7. To obtain the total overall annual probability of liquefaction, multiply the plot from Step 6 by $2\pi\bar{\lambda}R_i$ and integrate numerically the resulting function from $R_i = d_0$–$R_i = R_{max}$.

The procedure described previously assumes a circular earthquake source area extending from $R = d_0$–$R = R_{max}$. It is noteworthy herein that the same procedure could be applied for any size of an annular source area provided that the lower and upper limits of R are replaced by the adjusted (for focal depth) inner and outer radii of the annular area, respectively. If the annular

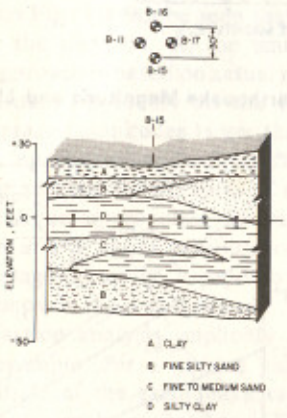

FIG. 6.—Subsurface Conditions at Example Site

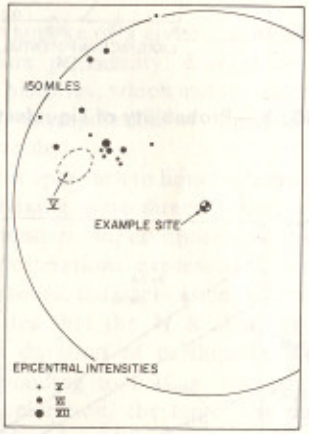

FIG. 7.—Seismic History from 1727–1966

source area is a fraction of a complete circle, the total probability computed in Step 7 should be multiplied by that fraction to obtain the probability of liquefaction corresponding to the annular source area.

Example

The soil profile considered herein is considered in Fig. 6, in which the silty sand layer extending from El. −26 to El. −38 is identified as a potentially liquefiable deposit and will therefore be the subject of this study. Inasmuch as the sand deposit is identified by four borings encompassing a circular area of about 30 ft (9.2 m) radius, the conclusions drawn from subsequent studies will be strictly valid only for the sand deposit described.

The water-table elevation as observed in the boreholes, varied from location to location. However, geophysical studies suggest that the water table is at about El. 0 ± 2 ft.

The density of the sand layer is moderately loose as indicated by the standard penetration data. The average blow count within the layer is estimated to be equal to 18 ± 2 blows/ft.

Seismicity of Region.—To estimate the seismic parameters, β and $\bar{\lambda}$, required for the risk analysis previously presented, it is essential to define a region around the site that is of seismic interest. Employing Eq. 15 the coefficient

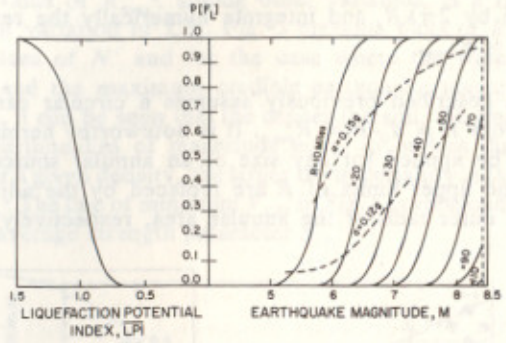

FIG. 8.—Probability of Liquefaction Versus Earthquake Magnitude and $\overline{\text{LPI}}$

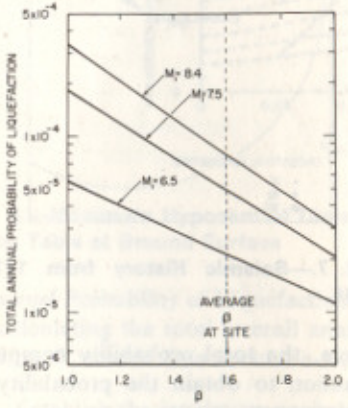

FIG. 9.—Total Annual Probability of Liquefaction Versus Magnitude-Frequency Parameter β

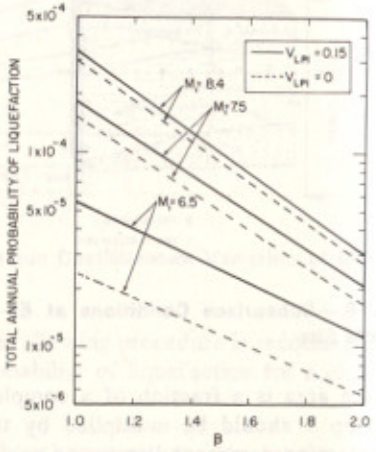

FIG. 10.—Influence of Coefficient of Variation of LPI, V_{LPI} on Computed Annual Probabilities of Liquefaction

of variation of $\overline{\text{LPI}}$ is calculated to be equal to 0.15. Substituting the value of V_{LPI} into Eq. 34 and assuming $M_1 = 8.4$, $R_{\max}$ is estimated to be 130 miles (210 km).

Fig. 7 shows the epicenters of some of the historic earthquakes of MMI intensities greater than or equal to V located within 150 miles (242 km) from the site. From this figure, it can be observed that during the period from 1727 to 1966, 16 earthquakes with epicentral intensities greater than V have occurred,

with epicenters located in the upper left quadrant of the 150-mile (242-km) radius circle. Therefore, it will be assumed that the future seismic activity in the region will also be confined to this quadrant and the earthquake source type is characterized by a "uniform" area with $d_0 = 10$ miles (16 km). Also, magnitude-frequency study of the 16 historic earthquakes yielded β values ranging from 1.35–2.0 with an average value equal to 1.6. The rate of earthquake occurrence $\bar{\lambda}$ is estimated to be equal to 4.0×10^{-6} earthquakes/yr/sq mile. Finally, the minimum magnitude of future earthquakes of engineering interest is assumed to be equal to 4.0 on the Richter scale.

The procedure recommended previously for computing the total annual probability of liquefaction was followed, assuming several different values of β, ranging from 1.0–2.0, and for different values of M_1 (8.4, 7.5, and 6.5). The conditional probabilities of liquefaction are plotted in Fig. 8. Fig. 9 shows the total annual probabilities of liquefaction for various values of β and M_1.

Discussion of Results

From Fig. 8 it can be seen that—for an earthquake of a given magnitude—the larger the distance, R, the smaller the failure probability. Insofar as the M & R approach is based on actual reported case histories, which include earthquake magnitudes up to 8.4 on the Richter scale, extrapolation of the analysis to earthquake magnitudes larger than 8.4 was avoided.

Among the reasons for formulating the M & R approach to liquefaction analysis was to account for duration of earthquake shaking more directly than do more conventional approaches. To verify this contention, superimposed on the plots shown in Fig. 8 are contours of constant accelerations expressed in terms of percentage of gravity. In order to plot these contours, the attenuation law proposed by Donovan (8) was assumed. Fig. 8 indicates that the M & R approach to liquefaction analysis implicitly accounts for duration of earthquake shaking. For example, for a ground shaking corresponding to 0.15 g, the larger the magnitude of the earthquake causing the acceleration, the larger the duration and the larger the probability of liquefaction. Also, from Fig. 8, it can be observed that a site may undergo different potential hazards depending upon the distance R and magnitude M of an earthquake. A distant but large magnitude earthquake causing a certain level of acceleration may have a far more damaging effect at a site as far as liquefaction is concerned than a close, but relatively smaller earthquake causing the same ground acceleration. The larger probability of failure associated with a large magnitude, but distant earthquake is explained by the long duration characteristic of large earthquakes.

The total overall annual probability results shown in Fig. 9 indicate that the smaller the assumed maximum earthquake magnitude the smaller the annual probability of liquefaction of the soil layer studied. For an average value for β of 1.6 at the site, the annual probability ranges between 2×10^{-5} and 8×10^{-5} depending upon M_1.

The total annual probability of liquefaction at the entire site may be obtained by summing the contributions of all the zones within the soil profile which are likely to liquefy. Such a summation can be performed using an equation similar to Eq. 2.

The key to the risk analysis presented herein is the plot of Fig. 3, which

describes the strength against liquefaction of the soil deposit under study. Inasmuch as the resistance function of Fig. 1 is empirically determined using limited field observations, uncertainties in the estimated strength $\bar{S}_c$ for soils of different densities are inevitable.

To determine the extent to which the computed total probabilities are sensitive to the variance of the strength parameter, $\bar{S}_c$, and consequently the variance of LPI, the preceding calculations were repeated with the variance of LPI reduced to zero. The results are plotted in Fig. 10. From this figure it can be observed that the degree of influence that Var $[\bar{S}_c]$ has on the total annual probability of liquefaction varies depending on the assumed maximum earthquake magnitude M_1. For the example studied herein, in which the average value of N' is equal to 18, the contribution of Var $[\bar{S}_c]$ (or Var [LPI]) to the probability of liquefaction is significant when $M_1 = 6.5$ and is relatively unimportant when $M_1 = 7.5$ or 8.4. However, it is important to note that for sites where the average value of N' is larger than 18, Var $[\bar{S}_c]$ may have significant influence on the total probability of liquefaction for assumed values of M_1 much greater than 6.5.

Conclusions

A methodology is proposed for studying the likelihood of ground failure by liquefaction. A probabilistic model is developed based on a new empirical method of analysis for liquefaction which employs earthquake magnitude and hypocentral distance. The model is later incorporated into a risk analysis for liquefaction. An example is included in which a risk analysis was conducted to evaluate the total probability of liquefaction of a layer of saturated fine silty sand.

It is recommended herein that further efforts be made to improve the criterion proposed and shown in Fig. 1 for liquefaction analysis based on the M & R approach. Additional case histories where liquefaction did not occur should be gathered and an improved statistical procedure should be devised which in the process of pattern recognition considers the bias in the case histories. Improvements in the criterion can also be introduced by considering the gradation characteristics of the soils studied in different case histories. Moreover, if a sufficiently large number of case histories is obtainable, the M & R approach to the interpretation of field data can be repeatedly followed using data corresponding to the same earthquake source type or from the same geographic area, or both, resulting in more refined criteria valid for a particular earthquake source mechanism or for a certain geographic region.

The methodology presented in this paper is an attempt to place analysis for liquefaction in the proper perspective. It is hoped that such an attempt may indicate the relative importance of the limitations or assumptions of the analysis presently used in practice, and may lead to alternate and more realistic approaches for the assessment of liquefaction potential at a site.

Acknowledgments

The work reported in this paper was part of a research program at the Massachusetts Institute of Technology under the general title of Seismic Design Decision Analysis. The research was sponsored by the Earthquake Engineering Program of NSF-RANN under grant GI-27955. The support of this organization is gratefully acknowledged. The writers gratefully acknowledge the advice and suggestions of E. H. Vanmarcke, C. A. Cornell, J. T. Christian, and D. Veneziano.

Appendix.—References

1. Algermissen, S. T., "The Problem of Seismic Zoning," *Building Practices for Distaster Mitigation*, Building Science Series 46, National Bureau of Standards, U.S. Department of Commerce, Washington, D.C., 1972.
2. Baecher, G. B., "Site Exploration: A Probabilistic Approach," thesis presented to the Massachusetts Institute of Technology, at Cambridge, Mass., in 1972, in partial fulfillment of the requirements for the degree of Doctor of Philosophy.
3. Benjamin, J. R., and Cornell, A. C., *Probability, Statistics, and Decision for Civil Engineers*, McGraw-Hill Book Co., Inc., New York, N.Y., 1970.
4. Castro, G., "Liquefaction and Cyclic Mobility of Saturated Sands," *Journal of the Geotechnical Engineering Division*, ASCE, Vol. 101, No. GT6, Proc. Paper 11388, June, 1975, pp. 551–569.
5. Christian, J. T., and Swiger, W. F., "Statistics of Liquefaction and SPT Results," *Journal of the Geotechnical Engineering Division*, ASCE, Vol. 101, No. GT11, Proc. Paper 11701, Nov., 1975, pp. 1135–1150.
6. Cornell, A. C., "Engineering Seismic Risk Analysis," *Bulletin*, Seismological Society of America, Vol. 54, No. 5, 1968.
7. Cornell, C. A., and Vanmarcke, E. H., "The Major Influences on Seismic Risk," *Proceedings of Fourth World Conference on Earthquake Engineering*, Santiago, Chile, Jan., 1969.
8. Donovan, N. C., "A Statistical Evaluation of Strong Motion Data Including the February 9, 1971 San Fernando Earthquake," presented at the Fifth World Conference on Earthquake Engineering, Rome, Italy, 1973.
9. Duke, C. M., and Leeds, D. J., "Responses of Soils, Foundations and Earth Structures to the Chilean Earthquakes of 1960," *Bulletin of the Seismological Society of America*, Vol. 53, No. 2, Feb., 1963.
10. "Earthquake Resistance Design for Civil Engineering Structures, Earth Structures and Foundations in Japan," Report, Japan Society of Civil Engineers, 1960.
11. Esteva, L., and Rosenblueth, E., "Spectra of Earthquakes at Moderate and Large Distance," *Society Mexico de Ing. Seismica*, Vol. II, No. 1, Mexico, 1964.
12. Kishida, H., "Characteristics of Liquefied Sands During Mino-Owari, Tohnarkai and Fukui Earthquakes," *Soils and Foundations*, Vol. IX, No. 1, 1969.
13. Kuribayashi, E., and Tatsuoka, F. "Brief Review of Liquefaction During Earthquakes in Japan," *Soils and Foundations*, Vol. 15, No. 4, Dec., 1975.
14. Lee, K. L., and Chan, K., "Number of Equivalent Significant Cycles in Strong Motion Earthquakes," *Proceedings of International Conference on Microzonation*, University of Washington, Seattle, Wash., Vol. 2, 1972.
15. Seed, H. B., and Idriss, I. M., "Analysis of Soil Liquefaction Niigata Earthquake," *Journal of the Soil Mechanics and Foundations Division*, ASCE, Vol. 93, No. SM3, Proc. Paper 5233, May, 1967, pp. 83–108.
16. Seed, H. B., and Lee, K. L., "Liquefaction of Saturated Sands During Cyclic Loading," *Journal of the Soil Mechanics and Foundations Division*, ASCE, Vol. 92, No. SM6, Proc. Paper 4972, Nov., 1966, pp. 105–134.
17. Seed, H. B., "Landslides During Earthquakes Due to Soil Liquefaction," *Journal of the Soil Mechanics and Foundations Division*, ASCE, Vol. 94, No. SM5, Proc. Paper 6110, Sept., 1968, pp. 1053–1122.
18. Seed, H. B., and Idriss, I. M., "Simplified Procedure for Evaluating Soil Liquefaction Potential," *Journal of the Soil Mechanics and Foundations Division*, ASCE, Vol. 97, No. SM9, Proc. Paper 8371, Sept., 1971, pp. 1249–1273.
19. Switzer, P., "Reconstructing Patterns from Sample Data," *Analysis of Mathematical Statistics*, Vol. 38, 1967.
20. Whitman, R. V., "Resistance to Soil Liquefaction and Settlement," *Soils and Foundations*, Vol. 11, No. 4, 1971.
21. Whitman, R. V., and Cornell, A. C., "Seismic Risk and Engineering Decision,"

C. Lomnitz and E. Rosenblueth, eds., Elsevier Scientific Publishing Co., New York, N.Y., 1976.
22. Yegian, M. K., "Risk Analysis for Earthquake-Induced Ground Failure by Liquefaction," thesis presented to the Massachusetts Institute of Technology, at Cambridge, Mass., in 1976, in partial fulfillment of the requirement for the degree of Doctor of Philosophy.